Spatial Fourier analysis of video photobleaching measurements

Principles and optimization

Tsong-Tseh Tsay* and Ken A. Jacobson[‡§]

*Biomedical Engineering Curriculum, School of Medicine, [‡]Laboratories for Cell Biology, Department of Cell Biology and Anatomy, [§]Lineberger Cancer Research Center; University of North Carolina at Chapel Hill, Chapel Hill, North Carolina 27599-7090 USA

ABSTRACT The major use of the fluorescence recovery after photobleaching (FRAP) technique is to measure the translational motion of the molecular components in various condensed media. In a conventional laser spot photobleaching experiment, a photomultiplier is used to measure the total brightness levels of the bleached region in the sample, so no spatial information can be directly obtained. In video-FRAP, a series of images after photobleaching is acquired, allowing the spatial character of the recovery to be determined; this permits direct detection of both anisotropic diffusion and flow. To utilize all of the available image data to determine the transport coefficients, a two-dimensional spatial Fourier transform analysis of the images after photobleaching was employed. The change in the transform between two time points reflects the action of diffusion during the interim. An important advantage of this method, which involves taking the ratio of image transforms at different time points, is that it does not require a specific initial condition to be created by laser photobleaching. The ability of the analysis to extract transport coefficients from computer-simulated diffusional recovery is assessed in the presence of increasing amounts of noise. Experimental data analysis from the diffusion of proteins in viscous solutions and from the diffusion of protein receptors on cell surfaces demonstrate the feasibility of the Fourier analysis to obtain transport coefficients from the video FRAP measurement.

INTRODUCTION

Conventional fluorescence recovery after photobleaching (FRAP)[1] using a focused laser spot has become a very useful tool to measure, on a microscopic scale, the translational mobility of components of membranes (Cherry, 1979), the cytoplasmic matrix (Luby-Phelps et al., 1988) and of polymer solutions (Barisas and Leuther, 1979) and films (Smith, 1982). The general technique (Peters et al., 1974; Edidin et al., 1976; Jacobson et al., 1976; Koppel et al., 1976) is based on laser photobleaching of a small region of a specimen labelled with fluorescent molecules. Following the photobleaching laser pulse, the recovery of fluorescence due to diffusion and/or flow from the surrounding region into the photobleached region is monitored with the same but much attenuated laser beam and a photomultiplier tube (PMT). The rate of recovery is related to the diffusion coefficient (D) or flow velocity of the fluorescent molecules in the membrane. A complete analysis of spot photobleaching data in terms of diffusion, uniform flow, and a combination of these processes has been presented by Axelrod and colleagues (1976). This form of the spot FRAP technique, however, does not inherently provide any spatial resolution to analyze the variation in two-dimensional fluorophore distributions during the recovery process. Elliptical beam photobleaching (Stolpen et al., 1988) was successfully developed to measure anisotropic diffusion. In general, however, video photobleaching (video-FRAP) has obvious advantages in both the analysis of anisotropic diffusion (Kapitza et al., 1985) and in tracing the movements of membranes (Lee et al., 1990) and cytoskeletal structures (Salmon et al., 1984; Wang, 1985; Sammak and Borisy, 1988) during cell motility phenomena. Replacing the PMT employed in conventional spot FRAP with low-light-level video imaging and digital image analysis (Reynolds, 1972; Arndt-Jovin et al., 1985; DiGuiseppi et al., 1985; Bright et al., 1986), the video FRAP technique records the entire intensity pattern after photobleaching, providing both temporal and spatial resolution. The analysis of a video photobleaching experiment is often semiquantitative or does not employ all of the data within the image (Kapitza et al., 1985). To more completely utilize all of the data, we have developed a spatial Fourier analysis for the video FRAP experiment which allows the extraction of isotropic and anisotropic diffusion coefficients.

We first discuss the theoretical basis of the analysis.

Address correspondence to Ken Jacobson Laboratories for Cell Biology, Department of Cell Biology and Anatomy, University of North Carolina, Chapel Hill, CB# 7090, 108 Taylor Hall, Chapel Hill, NC 27599-7090.

Dr. Tsay's present address is Beckman Laser Institute UC, Irvine, Irvine, CA 92715.

[1]*Abbreviations used in this paper: D*, diffusion coefficient; DMEM, Dulbecco's Modified Eagle Medium; FBS, fetal bovine serum; FRAP, fluorescence recovery after photobleaching; PBS, phosphate-buffered saline; PMT, photomultiplier tube; R-S-Con A, rhodamine-labeled succinylated concanavalin A; SNR, signal-to-noise ratio; TEM_{00}, transverse electromagnetic mode 00.

0006-3495/91/08/360/09 $2.00

Next, we apply this analysis to simulated diffusional transport recovery after photobleaching, varying the type and magnitude of noise. Such an analysis provides guidelines for the minimum signal-to-noise ratio in the images required for acceptable results. In addition, we discuss considerations for the optimization of spot size to the size of analyzed region and for the extraction of anisotropic diffusion information. The method of analysis is applied to diffusion of macromolecules in solution and to the diffusion of lectin receptors on the cell surface.

THEORETICAL BASIS FOR ANALYSIS

Diffusional transport is described by Fick's second law; in two dimensions, the partial differential equation becomes,

$$\frac{\partial}{\partial t} C(x, y, t) = D\nabla^2 C(x, y, t), \tag{1}$$

where C represents the concentration of fluorophore; D is the diffusion coefficient; x, y, and t have their conventional meanings; and ∇^2 is the two-dimensional Laplacian operator. The complexities of the initial and boundary conditions may make analytical solutions difficult or impossible to obtain and can consequently require intensive numerical methods (Crank, 1975).

The two-dimensional Fourier transform offers an independent means of solving Eq. 1 for an arbitrary initial condition requiring at the boundary that $C(x, y, t)$ is a constant as $(x, y) \rightarrow \pm\infty$. This is a reasonable approximation for macroscopic solutions and films and also for large cells if the photobleaching spot is relatively small. The Fourier transform of Eq. 1 is an ordinary differential equation and is given by,

$$\frac{\mathrm{d}}{\mathrm{d}t} \tilde{C}(u, v, t) = -4\pi^2 D(u^2 + v^2)\tilde{C}(u, v, t) \tag{2}$$

which has the solution

$$\tilde{C}(u, v, t) = \tilde{C}(u, v, 0)e^{-4\pi^2 D(u^2+v^2)t}, \tag{3}$$

where $\tilde{C}(u, v, t)$ represents the two-dimensional spatial frequency characterized by components u, v. In general the Fourier transform is a complex quantity. It can be represented by real and imaginary parts, or as an amplitude and phase angle. For diffusional transport phenomena, the amplitude changes as time elapses but the phase angle remains constant. In contrast, when pure flow occurs, the phase angle shifts as the time elapses but the amplitude remains constant. We ignored the phase of the transform because flows can be distinguished by inspection of the image.

Because the Fourier transform of the photobleach images depends on time in a simple way (Eq. 3), one can, in principle, obtain the D directly by a point-by-point division of the transforms obtained at two times after photobleaching:

$$R = \frac{\tilde{C}(u, v, t_2)}{\tilde{C}(u, v, t_1)} = e^{-4\pi^2 D(u^2+v^2)(t_2-t_1)} \tag{4}$$

and

$$D = \frac{-\ln R}{4\pi^2(u^2 + v^2)(t_2 - t_1)}. \tag{5}$$

Note that D is a constant and should not vary with spatial frequency.

Following Smith et al. (1979), for an anisotropic two-dimensional diffusion process, it is assumed that the D in the system depends on orientation but is independent of position and time. D can be expressed in tensor format and because D is constant, there exists coordinates X and Y in which D is diagonal:

$$D(\Theta) = D_{XX}\cos^2\Theta + D_{YY}\sin^2\Theta. \tag{6}$$

The angle Θ is between the wave vector specified by u and v and the positive u axis. Applying the Eq. 6 to Eq. 5, the anisotropic D is given by:

$$D\left(\tan^{-1}\frac{v}{u}\right) = \left(D_{XX}\frac{u^2}{u^2 + v^2} + D_{YY}\frac{v^2}{u^2 + v^2}\right) = \frac{-\ln R}{4\pi^2(u^2 + v^2)(t_2 - t_1)}. \tag{7}$$

Note that when $v = 0$,

$$D_{XX} = \frac{-\ln R}{4\pi^2 u^2(t_2 - t_1)} \tag{8}$$

and when $u = 0$,

$$D_{YY} = \frac{-\ln R}{4\pi^2 v^2(t_2 - t_1)}. \tag{9}$$

This allows the principal diffusion coefficients D_{XX}, and D_{YY}, to be extracted.

MATERIALS AND METHODS

Test specimens

Solutions of rhodamine-labeled, succinylated concanavalin A (R-S-Con A) (Vector Laboratories, Burlingame, CA) at ~63 μg/ml in viscous liquid glycerol (99.5% pure) (Fisher Scientific Company, Fair Lawn, NJ) were prepared. The glycerol solutions contained 1.2% water. A drop of the solution was placed on a microscope slide,

covered with a cover glass and pressed firmly to produce a thin slab of the sample. The diffusion coefficient (D) of the labeled solute could be varied by changing sample temperature from 0 to 37°C.

Before labeling lectin receptors on the cell surface, R-S-Con A was exhaustively dialyzed against phosphate-buffered saline (PBS) with Ca^{2+} and Mg^{2+} and centrifuged at 257,000 × g (Beckman TL-100 Ultracentrifuge, TLA-100.1 rotor; Beckman Instruments, Inc., Fullerton, CA) to remove any microaggregates. BG-9 cells (human foreskin fibroblasts) were cultured in Dulbecco's Modified Eagle Medium (DMEM) with 10% Fetal Bovine Serum (FBS) and penicillin/streptomycin on 12 × 12 mm cover slips. Subconfluent monolayers were rinsed with PBS three times and stained with R-S-Con A at 63 μg/ml for 10 min at room temperature. The stained monolayer culture slide was mounted with the cells down on a circular chamber machined into a metal slide which had been filled with PBS before mounting (Jacobson et al., 1984).

Video FRAP system

The video FRAP system used in our laboratory consists of a microscope and its accessories, a low-light-level camera, an argon ion laser, beam flag, a control box for controlling the camera shutter and beam flag, and a microcomputer with an image acquisition board and an array processor as previously described (Kapitza et al., 1985). The argon ion laser (model 164-07; Spectra-Physics, Mountain View, CA) was tuned to 514.5 nm in the TEM_{00} mode for rhodamine excitation. Generally, the camera employed was either a Dage model 66 ISIT (Michigan City, IN), or a Dage model 72 CCD optically coupled to a KS1381 microchannel plate (MCP) intensifier (Video Scope International Ltd., Washington, D.C.). Gains of the cameras and intensifier were manually controlled. A slow scanned CCD (STAR I; Photometrics, Tucson, AZ) was employed for the diffusion of protein receptors on the cell surfaces.

The video-digitizing board (Datacube, Peabody, MA) consisted of 768 horizontal pixels × 512 vertical pixels × 8 bit deep frame store utilizing a 14.3 MHz, 8 bit A/D converter. Video images of 256 × 256 pixels were digitized to 256 gray level resolution, captured in the frame buffer and were averaged for up to 256 frames. The host computer was a MICRO/PDP-11 (Digital Equipment Corporation, Maynard, MA) with 512K memory, hard disk, and floppy diskette driver (Scientific Micro Systems, Mountain View, CA). The computer also sent signals

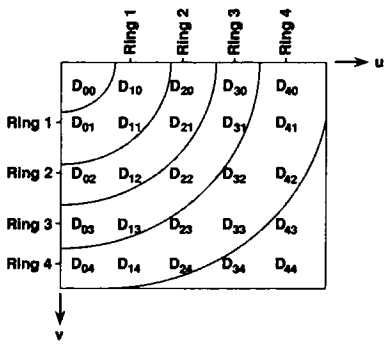

FIGURE 1 Spatial frequency (u, v) assignment to "rings" for azimuthal averaging. $D(u, v)$ is the calculated from Eq. 5 at spatial frequency (u, v). $D_{ring\ 1} = 1/3\ (D_{10} + D_{11} + D_{01})$; $D_{ring\ 2} = 1/4\ (D_{20} + D_{21} + D_{12} + D_{02})$; $D_{ring\ 3} = 1/5\ (D_{30} + D_{31} + D_{22} + D_{13} + D_{03})$; $D_{ring\ 4} = 1/9\ (D_{40} + D_{41} + D_{42} + D_{32} + D_{33} + D_{23} + D_{24} + D_{14} + D_{04})$.

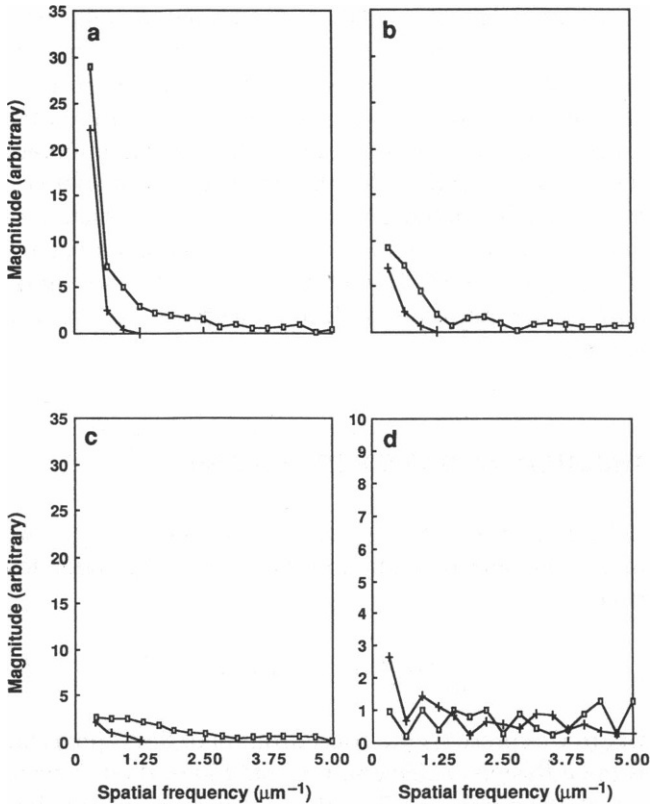

FIGURE 2 Frequency amplitude spectra of various diameter "ideal" bleached spots and their surroundings immediately after bleaching and after simulated diffusional recovery occurs for 0.2 min with D = 2.3 × 10^{-9} cm^2/s. Bleached spot was set to 100 grey levels while background was set to 150 grey levels. (a) Frequency spectrum of ideal 32 pixel diameter bleached spot right after photobleaching (□); and after partial recovery (+); (b) Frequency spectrum of ideal 16 pixel diameter bleached spot right after photobleaching (□); and after partial recovery (+). (c) Frequency spectrum of ideal 8 pixel diameter bleached spot right after photobleaching (□); and after partial recovery (+). (d) Typical frequency spectrum of Gaussian noise (□), (standard deviation of the noise is σ = 10); frequency spectrum of typical fluorescent image (SNR = 15 and is defined as in Table 8). (Figures correspond to frequency spectrum along u axis. For reference, Ring 1 corresponds to u = 0.3125 μm^{-1}, Ring 2 corresponds to u = 0.625 μm^{-1}, Ring 3 corresponds to u = 0.9375 μm^{-1}.)

to a relay-operated beam flag which blocked the laser beam at all times except during photobleaching and to a shutter for camera protection during the photobleaching light pulse. A SKYMNK array processor from Sky Computers (Lowell, MA) in the MICRO/PDP-11 was used to accelerate Fourier transform image processing. This array processor was limited to handling 64 × 64 pixel images.

Measurements of diffusion coefficients by conventional FRAP were performed as a reference as described previously (Ishihara et al., 1987).

Data acquisition and analysis

A video FRAP program was written in the Video Facility of the Department of Cell Biology and Anatomy, UNC-CH. Data acquisition

starts by storing a prephotobleaching image for reference. Next, the image shutter closes to protect the light-sensitive camera during the photobleaching step. This is followed by an intense, short laser pulse which bleaches the fluorophore population. After a few milliseconds delay, the camera shutter opens to acquire the first postbleach image. A series of images are taken at predefined time intervals to record the fluorescence recovery. The final image is acquired after an extended time to record the reequilibrated state after the photobleaching step.

D's can be calculated by the decay of individual spatial frequency components as recovery proceeds (Eq. 5). High-frequency components decay more quickly than the low-frequency components and are subject to more noise contamination. We averaged the D's obtained from approximately equivalent spatial frequencies defined by "rings" in Fourier space to provide some data smoothing for the case of isotropic diffusion. This amounts to an azimuthal averaging in the transform space to obtain more precise results. The assignment of spatial frequencies (u, v) to defined rings $(1, 2, 3, 4, \ldots)$ is illustrated in Fig. 1. For example, D_{2_1} represents the diffusion coefficient calculated at the spatial frequency defined by $u = 2, v = 1$, and D_{2_1} is assigned to Ring 2.

Computer simulation

Diffusional recovery based on particles moving on a 64 × 64 square lattice was simulated by computer (for principles, see Berg, 1983). The principle of the computer simulation can be explained as follows. At each lattice point a given large number of particles represents membrane protein molecules at that point. Isotropic random diffusion of molecules is simulated by moving these particles to one of the neighboring lattice points in both x and y directions. At the boundary of the square lattice, outward movements of particles were reflected by the boundary. The simulation of anisotropic random diffusion is similar to that of isotropic random diffusion except the probabilities of movement in the x and y directions are different. In one diffusion step operation, all the particles are moved randomly by one lattice constant. This operation was repeated successively to simulate the true evolution of a distribution under the influence of diffusion. The interval (τ) between operations was calculated according to the equation $\tau = \delta^2/4D$, where δ represents one diffusive step length (lattice constant). We began with an ideal photobleached image to test the accuracy of the simulation algorithm. The ideal image was generated with uniform background (gray level = 150) and a bleached spot (16 pixels in diameter, gray level = 100). The diffusional recovery into this spot was then simulated and the diffusion coefficient calculated by Eq. 5 was compared with the D employed in the simulated recovery.

To study the effects of noise on this Fourier transform analysis, photon noise was added to the ideal photobleached image. Although photon noise has a Poisson distribution, for large photon fluxes, Gaussian noise represents a good approximation to Poisson noise (Bevington, 1969). We therefore added different magnitudes of Gaussian noise to the simulated recovery images to estimate how image noise affected the analysis. The magnitude of the noise was characterized by σ, the standard deviation in gray level about the mean. In some simulations, we also superimposed the actual noise in a fluorescent image recorded with a given detector on the artificial bleached spot.

TABLE 1 **Diffusion coefficients extracted from simulated recoveries into different size bleached spots***

Spot diameters (in pixel)	32	16	8
D ($\times 10^9\ cm^2/s$)	2.32 ± 0.61	2.31 ± 0.42	2.10 ± 1.20

*Simulated $D = 2.3 \times 10^{-9}$ cm^2/s. Gaussian noise with $\sigma = 10.0$ in gray level was generated by computer and added to the uniform background (150 gray levels) and bleaching spot (100 gray levels); the bleached spot sizes were 8, 16, and 32 pixels in diameter. The spot size of 16 pixels in diameter and other conditions also apply to the data in Tables 2 and 4. The diffusion coefficients are calculated by azimuthal averaging the D's calculated from Ring 2 spatial frequencies as defined in Fig. 1 (see text for details).

RESULTS AND DISCUSSION

Basic considerations in experimental design as determined by simulations of the recovery process

Size of photobleaching spot in relation to size of analysis region

A number of basic factors must be considered in setting up this form of the video FRAP measurement. Optimization of these factors can be quantitatively evaluated using artificial images derived from a computer simulation of diffusional recovery into a spot created by "photobleaching". First, we consider the size of the photobleached spot in relation to the analysis region. For reference, the Fourier amplitude spectra of the image of large, medium, and small spots and their surroundings are given in Figs. 2 *a–c*, respectively, together with the spectra after recovery has proceeded for 12 s. In relation to the size of the analysis region the spot must not be too large, otherwise the condition that fluorescence at the boundary of the specimen be essentially unchanged after photobleaching will not hold. On the other hand, if the spot is too small, the amplitude

TABLE 2 **Diffusion coefficients extracted after different % recoveries have occurred**

% Recovery*	11	29	44	78	89
D ($\times 10^9\ cm^2/s$)	3.01 ± 0.40	2.59 ± 0.16	2.55 ± 0.11	2.15 ± 0.25	1.04 ± 0.15

*% Recovery is defined as: [(gray level of central pixel after partial recovery − 100)/(150 − 100)] × 100%; simulated $D = 2.3 \times 10^{-9}$ cm^2/s; Gaussian noise ($\sigma = 10$) was added to the simulated images.

TABLE 3 **Fourier analysis of noise-free simulated recovery for $D = 2.3 \times 10^{-9}$ cm²/s**

	Recovery time	% Recovery*	Ring 1	Ring 2	Ring 3
	1 s	11%	2.30	2.22	2.38
	2 s	20%	2.37	2.26	2.34
D	3 s	29%	2.25	2.24	2.32
($\times 10^9$ cm²/s)	6 s	44%	2.29	2.29	2.41
	12 s	62%	2.22	2.36	2.28
	24 s	78%	2.29	2.25	1.62

*% Recovery is defined as in Table 2.

associated with the spatial frequencies composing the image of the spot will be smaller (Fig. 2 *c*) and tend to be contaminated with noise (Fig. 2 *d*) to a greater extent. We have found, as a useful rule of thumb, that the spot diameter should be ~one-fourth of the linear dimension of the analyzed image. Note that according to the Eq. 3, diffusional transport can be represented as the product of the initial spectrum of the image of photobleached specimen and an exponential term acting as filter. This term quickly filters out the high-frequency components leaving only the low-frequency components (see the spectra of bleached spots after diffusional recovery in Figs. 2 *a–c*).

Diffusion coefficients extracted from the Fourier analysis of simulated recovery for several different spot sizes are given in Table 1. Note that the smallest spot yields a slightly lower D and a higher standard deviation. Comparing Figs. 2 *c* and 2 *d*, one sees that noise ($\sigma = 10$) becomes an appreciable contaminant when the smallest spot size is employed leading to greater uncertainty in the determination of D. For the medium and large bleached spots, there is good agreement between the calculated D and the D employed in the simulation, although for large spots (32 pixels in diameter) adherence to the boundary condition is dubious (see above).

Timing of images of the recovery process

Images of the recovery process must be taken within a certain time range (i.e., related to % recovery) after photobleaching for optimum extraction of transport information. Considering that the first image is taken shortly after photobleaching, if the second postbleach image is taken too soon after the first, the low frequencies (which carry most of the usable information) will not have changed enough resulting in an imprecise calculation of D. On the other hand, if too much time has elapsed between first and second images, the second image contains little useful information as recovery is nearly complete. The analysis of simulated data shows these effects (Table 2). The most reliable D's are obtained when the second image is taken after between 30 and 80% of the fluorescence recovery has occurred.

Effects of image noise on the analysis

A crucially important factor for the success of this analysis is the SNR in the image. In noise-free simulations, the analysis returned the D put into the simulation independent of the spatial frequencies employed for the analysis (in terms of ring number) or the time elapsed between postbleach images (Table 3). An error only occurs close to complete recovery for high-frequency components (see Ring 3 at 78% recovery) and is due to the quantized nature of the digitized image.

Gaussian noise generated from a computer was then added to each image characterized by $\sigma = 10$ (standard deviation) to provide a first estimate of how the precision of the analysis depends on image noise. The results are shown in Table 4. This analysis shows that spatial frequencies in Rings 1 and 2 provide the best results. Information in the higher spatial frequencies (Ring 3) is quickly eroded by diffusion so that by the time recovery is more than half complete, analysis with ring 3 frequencies is no longer reliable. Ring 1 is less reliable only for short times after bleaching when little change in the low spatial frequencies has occurred; at times where recovery is nearly complete, Ring 1 frequencies are best for analysis. Overall, in terms of precision of the analysis, Ring 2 frequencies appear optimal for analysis. The deterioration in the precision of D's extracted from Ring

TABLE 4 **Fourier analysis of simulated recovery with Gaussian noise, $\sigma = 10.0$, for $D = 2.3 \times 10^{-9}$ cm²/s**

	Recovery time	% Recovery*	Ring 1	Ring 2	Ring 3
	1 s	11%	2.14 ± 2.70	3.01 ± 0.40	2.40 ± 0.97
	2 s	20%	1.86 ± 1.00	2.58 ± 0.21	2.19 ± 0.62
D	3 s	29%	2.21 ± 0.95	2.59 ± 0.16	2.48 ± 0.58
($\times 10^9$ cm²/s)	6 s	44%	2.28 ± 0.52	2.55 ± 0.11	1.99 ± 0.29
	12 s	62%	2.23 ± 0.31	2.68 ± 0.12	1.23 ± 0.12
	24 s	78%	2.33 ± 0.25	2.15 ± 0.25	0.63 ± 0.49

*% Recovery is defined as in Table 2.

TABLE 5 **Effect of image signal-to-noise ratio on precision of extracted *D*'s***

σ	0	5	10	20
SNR	∞	30	15	7.5
D ($\times 10^9 cm^2/s$)	2.30 ± 0	2.38 ± 0.06	2.55 ± 0.11	2.71 ± 0.76

*Recovery simulated using $D = 2.3 \times 10^{-9}$ cm²/s; D calculated from Ring 2 frequencies after 44% recovery.

2 frequencies as image SNR decreases is shown in Table 5.

The simulation can be made more realistic by superimposing the actual noise from a fluorescent image. The SNR of the particular fluorescent image, defined as the average in the gray levels of a central 25 × 25 pixel region divided by the standard deviation, was ~17. The test image employed was that taken of R-S-Con A in glycerol solution using an ISIT camera. We superimposed artificially bleached spots on the test image to simulate a time right after photobleaching and a partially recovered image. The bleached spot immediately after photobleaching was generated by subtracting a uniform value (gray level = 50; diam = 16 pixels) from a specific region in the fluorescent image. The partially recovered spot was generated by subtracting from the same sized region in the original fluorescent image, intensity values due to partial diffusional recovery as simulated by computer. The extracted D of (2.51 ± 0.63) × 10^{-9} cm²/s, is somewhat less precise compared with D of (2.55 ± 0.11) × 10^{-9} cm²/s in the Table 5 (SNR = 15). Presumably, this is due to the fact that camera noise has higher amplitude than simple white noise at the low spatial frequencies where the analysis is performed (see Fig. 2 *d*).

TABLE 6 **Anisotropic recovery***

		Diffusion coefficient		
Recovery time	% Recovery‡	D_{20}	D_{02}	D_{03}
s		$\times 10^9 cm^2/s$	$\times 10^{10} cm^2/s$	$\times 10^{10} cm^2/s$
1	6.7%	3.15 ± 1.04	12.77 ± 13.39	8.24 ± 15.43
2	11.1%	2.67 ± 0.57	7.20 ± 6.73	5.01 ± 7.83
3	15.6%	2.48 ± 0.42	5.72 ± 4.54	4.10 ± 5.34
6	28.9%	2.34 ± 0.28	4.17 ± 2.35	3.37 ± 2.90
12	42.2%	2.26 ± 0.25	3.16 ± 1.25	2.86 ± 1.67
24	57.8%	2.03 ± 0.31	2.72 ± 0.71	2.77 ± 1.16
48	73.3%	1.42 ± 0.28	2.60 ± 0.47	2.83 ± 1.03
96	82.2%	0.73 ± 0.14	2.84 ± 0.42	2.00 ± 0.45

*Fourier analysis of simulated recovery image with superimposed Gaussian noise ($\sigma = 10.0$) for $D_{XX} = 2.3 \times 10^{-9}$ cm²/s and $D_{YY} = 2.30 \times 10^{-10}$ cm²/s.
‡% Recovery is defined as in Table 2.

TABLE 7 **Comparison of diffusion coefficients obtained by video FRAP and conventional FRAP for R-S-Con A in an aqueous glycerol solution* at various temperatures**

	Diffusion coefficient ($D \times 10^{-9} cm^2/s$)			
		Video FRAP‡		
Temp	Spot FRAP	Ring 1	Ring 2	Ring 3
°C				
0	1.24 ± 0.14	2.44 ± 0.26	1.06 ± 0.19	0.07 ± 0.15
10	1.86 ± 0.40	2.46 ± 0.59	1.90 ± 0.73	0.75 ± 0.89
24	2.25 ± 0.32	3.20 ± 0.32	2.52 ± 0.36	0.58 ± 0.50
37	4.32 ± 0.30	9.33 ± 1.65	3.77 ± 1.25	0.32 ± 1.16

*63 μg/ml R-S-Con A in 98.8% glycerol solution.
‡Analysis after recovery 35% complete.

ANALYSIS OF ANISOTROPIC DIFFUSION

Anisotropic diffusion was also simulated using the same conditions as described in Table 4 except that $D_{XX} = 2.3 \times 10^{-9}$ cm²/s and $D_{YY} = 2.3 \times 10^{-10}$ cm²/s. The results are shown in Table 6. In this case, recovery is dominated by the higher diffusion coefficient ($D_{XX} = 2.3 \times 10^{-9}$ cm²/s) and reasonable values for D_{XX} can be extracted for recovery in the range of 10–70% (D_{XX} is evaluated at ring two and hence termed D_{20}). The lower diffusion coefficient in the y direction means that spatial frequencies along the v axis will change much more slowly. Indeed, D_{YY} calculated from either ring 2 or ring 3 is inaccurate until recovery approaches nearly 50%. From 50 to 80% recovery, the extracted D_{YY} is in reasonable agreement with the simulated value ($D_{YY} = 2.3 \times 10^{-10}$ cm²/s). Thus, for the condition that $D_{YY} = 0.1\ D_{XX}$, the principle D's characterizing anisotropic transport can be extracted after recovery is ~50% complete. This simulation indicates that the Fourier analysis is capable of

TABLE 8 **Effect of image SNR* on precision of the Fourier analysis**

	Diffusion coefficient ($D \times 10^{-9} cm^2/s$)	
Image SNR	video-FRAP‡	spot-FRAP
28	2.66 ± 0.66	2.42 ± 0.17
15	3.12 ± 2.25	2.88 ± 0.36

*Image SNR defined as: SNR = mean grey level of a central 25 × 25 pixel region/std. deviation of the region in grey level.
‡Analysis after recovery 40% complete.

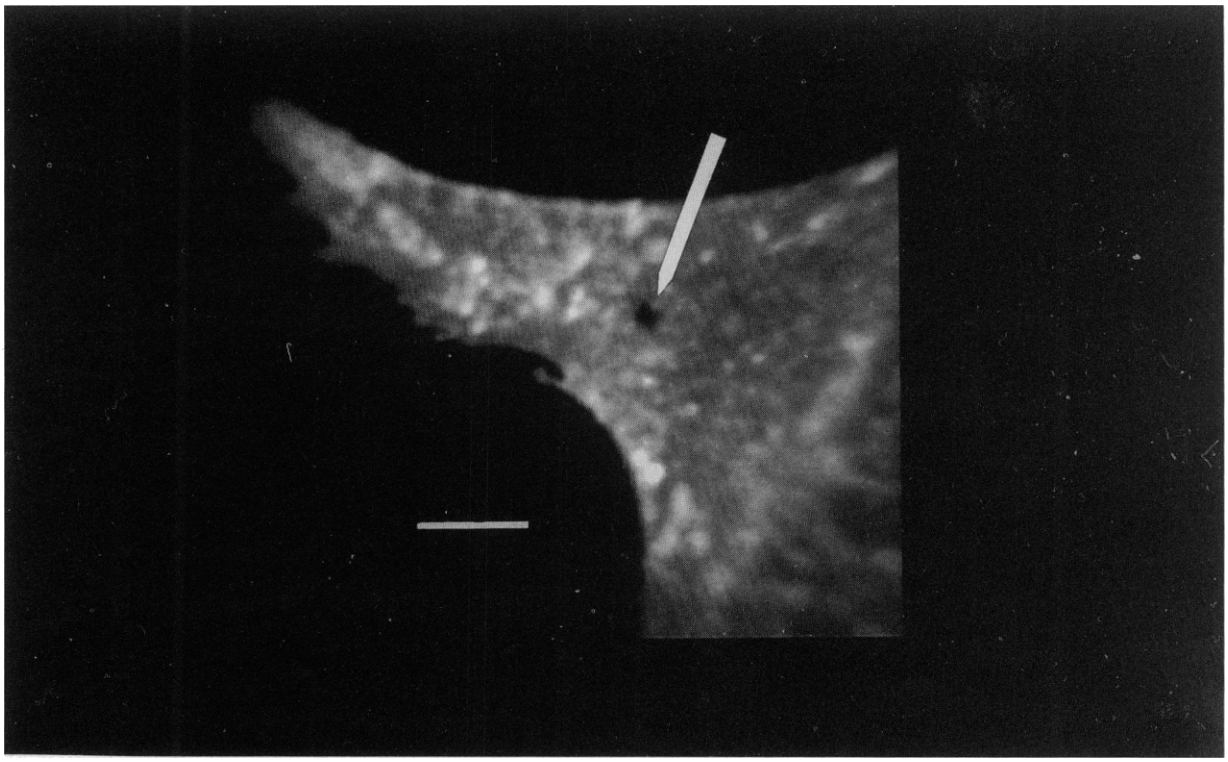

FIGURE 3 Typical fibroblast cell labeled with the lectin R-S-Con A lectin immediately after a spot was photobleached (*arrow*). The image was acquired using a slow scan CCD (STAR I; Photometrics, Tucson, AZ) under manual mode. The acquisition time was 10 s; the camera head was cooled down to −45°C; and the gain and bin setting were equal to 1. Bar equals 10 μm.

determining anisotropic D's differing by at least an order of magnitude.

EXPERIMENTAL RESULTS

Macromolecular solutions

The Fourier analysis method was employed to determine the translational D of rhodamine succinyl-concanavalin A (R-S-Con A) in viscous glycerol solutions. The results of the analysis were compared with results obtained by conventional spot photobleaching (Table 7). This study demonstrates good agreement between the Fourier analysis of video FRAP data and conventional spot photobleaching data at various temperatures, provided that spatial frequencies in Ring 2 are analyzed (Table 7). However, the Fourier analysis requires high image signal-to-noise ratios to achieve acceptable precision even after azimuthally averaging the results in different rings. This is shown by comparing the video FRAP results to those obtained by conventional spot bleaching for two image SNR (Table 8). Essentially, this requirement for high SNR in the video FRAP experiment reflects the difference between the imaging and the integrating (spot bleaching) techniques.

Diffusion on the cell surface

The D of lectin receptors on the surface of BG-9 fibroblasts was obtained by both conventional and Fourier transform video FRAP methods. Cells were labeled with 63 μg/ml R-S-Con A at room temperature for 10 min. Fig. 3 shows a typical image of fibroblast cell after photobleaching, acquired by the slow scanned CCD. Any immobile fraction, whether spatially variegated or not, is not analyzed by the Fourier method. This component was removed by subtracting the image after completed recovery from the other post-bleach images; the Fourier transform is then only performed on difference images whose content represents the diffusing population. This study also demonstrates the agreement between the two methods. For conventional spot bleaching $D = (7.5 \pm 0.7) \times 10^{-11}$ cm^2/s and for the Fourier transform video FRAP technique, $D = (7.5 \pm 4.9) \times 10^{-11}$ cm^2/s, using ring 2 data after recovery was 40% complete.

SUMMARY AND OUTLOOK

This paper demonstrates the feasibility of Fourier analysis to obtain transport coefficient from a video FRAP measurement. Such experiments are usually conducted using a digitized fluorescence microscope equipped with a laser for photobleaching (Kapitza et al., 1985), but video photobleaching is convenient using the laser-scanning confocal microscope (Cooper et al., 1990) and the Fourier analysis will be applicable to data taken on these instruments. It is clear that the analysis will be most useful in images of specimens which provide a high SNR. Thus, for example, polymer films which can be highly doped with a fluorescent probe could be analyzed by this method. The general strategy of taking only two or three post bleach images with a single readout per image and with high excitation energy to improve image SNR should be considered because of the absolute requirement of high SNR for successful analysis. In this case, essentially all the available fluorescence could be obtained before the fluorophores were totally bleached (Jovin et al., 1990).

Many biological specimens, in which the cell surface or cytoplasmic matrix is analyzed, will be characterized by a labeled population exhibiting more than one diffusion coefficient. The problem of multiple diffusion coefficients can, in principle, be attacked by obtaining a number of postbleach images to characterize a multiexponential decay described by a summation of terms of the form of the right side of Eq. 3. In the case of a single diffusing species, obtaining more postbleach images and fitting the exponential should lead to a more precise analysis. In the case of multiple diffusion coefficients, a curve-fitting approach could be employed; of course, confidence in this approach would increase as the specimen SNR increased.

We wish to acknowledge the contribution of Dr. Richard T. Inman who originally suggested this analysis for video photobleaching and the helpful comments of the referees.

This work was supported by National Institutes of Health grant GM41402.

Received for publication 2 January 1991 and in final form 23 April 1991.

REFERENCES

Arndt-Jovin, D. J., M. Robert-Nicoud, S. J. Kaufman, and T. M. Jovin. 1985. Fluorescence digital imaging microscopy in cell biology. *Science (Wash. DC).* 230:247–256.

Axelrod, D., D. E. Koppel, J. Schlessinger, E. Elson, and W. W. Webb. 1976. Mobility measurement by analysis of fluorescence photobleaching recovery kinetics. *Biophys. J.* 16:1055–1069.

Barisas, G., and M. Leuther. 1979. Fluorescence photobleaching recovery measurement of protein absolute diffusion constants. *Biophys. Chem.* 10:221–229.

Berg, H. C. 1983. Random Walks in Biology. Princeton University Press, Princeton, NJ. 130–132.

Bevington, P. R. 1969. Data Reduction and Error Analysis for The Physical Sciences. McGraw-Hill, Inc., New York. 36.

Bright, G. R., and D. L. Taylor. 1986. Imaging at low light level in fluorescence microscopy. *In* Applications of Fluorescence in the Biomedical Sciences. A. R. Liss, New York. 257–288.

Cherry, R. J. 1979. Rotational and lateral diffusion of membrane proteins. *Biochim. Biophys. Acta.* 559:289–327.

Cooper, M. S., A. H. Cornell-Bell, A. Chernjavsky, J. W. Dani, and S. J. Smith. 1990. Tubulovesicular processes emerge from trans-Golgi cisternae, extend along microtubules, and interlink adjacent trans-Golgi elements into a reticulum. *Cell.* 61:135–145.

Crank, J. 1975. The Mathematics of Diffusion. Clarendon Press, Oxford, U.K. 137–159.

DiGuiseppi, J., R. T. Inman, A. Ishihara, K. A. Jacobson, and B. Herman. 1985. Applications of digitized fluorescence microscopy to problems in cell biology. *Biotechniques.* 3:394–403.

Edidin, M., Y. Zagyanski, and T. Lardner. 1976. Measurement of membrane protein lateral diffusion in single cells. *Science (Wash. DC).* 191:466–468.

Ishihara, A., Y. Hou, and K. Jacobson. 1987. The Thy-1 antigen exhibits rapid lateral diffusion in the plasma membrane of rodent lymphoid cells and fibroblasts. *Proc. Natl. Acad. Sci. USA.* 84:1290–1293.

Jacobson, K., Z. Derzko, E-S Wu, Y. Hou, and G. Poste. 1976. Measurement of the lateral mobility of cell surface components in single, living cells by fluorescence recovery after photobleaching. *J. Supramol. Struct.* Alan R. Liss, New York. 5:565–576.

Jacobson, K., D. O'Dell, and J. August. 1984. Lateral diffusion of an 80,000 glycoprotein in the plasma membrane of murine fibroblasts: relationships to cell structure and function. *J. Cell Biol.* 99:1624–1633.

Jovin, T. M., D. J. Arndt-Jovin, G. Marriott, R. M. Clegg, M. Robert-Nicoud, and T. Schormann. Distance, wavelength and time: the versatile 3rd dimensions in light emission microscopy. *Optical Microscopy for Biology.* B. Herman and K. Jacobson, editors. Wiley-Liss, New York. 575–602.

Kapitza, H. G., G. McGregor, and K. A. Jacobson. 1985. Direct measurement of lateral transport in membranes by using time-resolved spatial photometry. *Proc. Natl. Acad. Sci. USA.* 82:4122–4126.

Koppel, D. E., D. Axelrod, J. Schlessinger, E. L. Elson, and W. W. Webb. 1976. Dynamics of fluorescence marker concentration as a proble of mobility. *Biophys. J.* 16:1315–1329.

Lee, J., M. Gustafsson, K-E. Magnusson, and K. Jacobson. 1990. The direction of membrane lipid flow in locomoting polymorphonuclear leukocytes. *Science (Wash. DC).* 247:1229–1233.

Luby-Phelps, K., F. Lanni, and D. L. Taylor. 1988. The submicroscopic properties of cytoplasm as a determinant of cellular function. *Annu. Rev. Biophys. Biophys. Chem.* 17:369–396.

Peters, R., J. Peters, K. H. Tews, and W. Baehr. 1974. A microfluorimetric study of translational diffusion in erythrocyte membranes. *Biochim. Biophys. Acta.* 367:282–294.

Reynolds, G. T. Photosensitive devices applied to X-ray diffraction studies and microscopic observations of bioluminescence. *Q. Rev. Biophys.* 5:295–347.

Salmon, E. R., R. J. Leslie, W. N. Saxton, M. L. Karrow, and J. R. McIntosh. 1984. Spindle microtubule dynamics in sea urchin embryos: analysis using a fluorescein-labelled tubulin and measurements of fluorescence redistribution after laser photobleaching. *J. Cell Biol.* 99:2165–2174.

Sammak, P. J., and G. G. Borisy. 1988. Direct observation of microtubule dynamics in living cells. *Nature (Lond.).* 332:724–726.

Smith, B. A. 1982. Measurement of diffusion in polymer films by fluorescence redistribution after pattern photobleaching. *Macromolecules.* 15:469–472.

Smith, B. A., W. R. Clark, and H. M. McConnell. 1979. Anisotropic molecular motion on cell surfaces. *Proc. Natl. Acad. Sci. USA.* 76:5641–5644.

Stolpen, A. H., J. S. Pober, C. S. Brown, and D. E. Golan. 1988. Class I major histocompatibility complex proteins diffuse isotropically on immune interferon-activated endothelial cells despite anisotropic cell shape and cytoskeletal organization: application of fluorescence photobleaching recovery with an elliptical beam. *Proc. Natl. Acad. Sci. USA.* 85:1844–1848.

Wang, Y-L. 1985. Exchange of actin subunits at the leading edge of living fibroblasts: possible role of treadmilling. *J. Cell Biol.* 101:597–602.